Title

Airborne Asian dust: case study of long-range transport and implications for the detection of volcanic ash

Journal

Weather and Forecasting, 18(2)

ISSN

0882-8156

Authors

Simpson, James J
Hufford, G L
Servranckx, R
et al.

Publication Date

2003-04-01

Peer reviewed

Airborne Asian Dust: Case Study of Long-Range Transport and Implications for the Detection of Volcanic Ash

J. J. SIMPSON

Digital Image Analysis Laboratory, Scripps Institution of Oceanography, University of California, San Diego, La Jolla, California

G. L. HUFFORD

Aviation Technology Center, University of Alaska, Anchorage, Anchorage, Alaska

R. SERVRANCKX

Canadian Meteorological Centre, Meteorological Service of Canada, Montreal, Quebec, Canada

J. BERG

Digital Image Analysis Laboratory, Scripps Institution of Oceanography, University of California, San Diego, La Jolla, California

D. PIERI

Jet Propulsion Laboratory, California Institute of Technology, Pasadena, California

(Manuscript received 24 April 2002, in final form 19 August 2002)

ABSTRACT

The transport of fine-grained Asian dust from its source (e.g., the Gobi Desert, Mongolia) to North America is a common springtime phenomenon. Because of its chemical composition (silicon, iron, aluminum, and calcium) and its particle size distribution (mean aerodynamic diameter 2–4 μm), Asian dust produces a negative signal in the split-window $T_4 - T_5$ algorithm, as does airborne volcanic ash. The split-window algorithm is commonly used by operational volcanic ash advisory centers. Thus, it is important to find ways to differentiate between airborne Asian dust and airborne volcanic ash. Use of Total Ozone Mapping Spectrometer aerosol and sulfur dioxide indices, in conjunction with the split-window method, can mitigate the possibility of a false airborne volcanic ash alarm. Asian dust also is important for other reasons. Thus, meteorological agencies should monitor it because 1) it can be transported thousands of kilometers from its source region and thus is of global interest (e.g., effects on radiative forcing) and 2) fine-grain particles pose a potentially serious public health hazard.

1. Introduction

Dust clouds over the world's deserts and sand seas (e.g., Gobi, Mongolian, Sahara) form when friction from surface winds (>5 m s^{-1}) entrains and lifts dust particles into the atmosphere (Gillette 1978), especially when agitated by sand-grain saltation within and through the local viscous boundary layer (Bagnold 1941). Global transport of desert dust from its source points 1) to the North Pacific Ocean atmosphere (Prospero et al. 1989; Husar et al. 2001), 2) over the Mediterranean Sea (Chester et al. 1984; Dulac et al. 1992), and 3) over the tropical North Atlantic Ocean (Talbot et al. 1986; Ozloy et al. 2001) is documented well. The resultant atmospheric particles have been studied within the contexts of radiative forcing and climate (e.g., Myhre and Stordal 2001), carriers in the biogeochemical cycles of crustal elements (e.g., Chadwick et al. 1999), and public health (Schwartz et al. 1999).

This paper 1) reviews some satellite-based retrievals of aerosol, 2) presents a case study of two recent Asian dust events-including detection from satellites and modeling of the atmospheric transport, 3) examines the potential effects of desert dust on the performance of the operational split-window airborne volcanic-ash detection algorithm, and 4) suggests possible ways of differentiating dust from volcanic ash using satellite data. Pressure analyses are in the original projection provided by The National Oceanic and Atmospheric Administration (NOAA). Geostationary Operational Environmental Satellite (GOES) data are in satellite projection,

Corresponding author address: J. J. Simpson, Digital Image Analysis Laboratory, Scripps Institution of Oceanography, University of California, San Diego, La Jolla, CA 92093-0237.
E-mail: jsimpson@ucsd.edu

which is the projection given to most forecasters. Moreover, given the size of GOES data, no single standard map projection (e.g., polar stereographic, Mercator) is appropriate.

2. Satellite-based retrievals

a. Split-window detection of airborne volcanic ash

Because most active volcanoes are in remote and seismically uninstrumented sites, operational detection of airborne volcanic ash by volcanic ash advisory centers (VAACs) has relied heavily on satellite remote sensing using the split-window method. It evaluates the Advanced Very High Resolution Radiometer or equivalent 11-μm (T_4) and 12-μm (T_5) brightness temperature (BT) difference ($\Delta T = T_4 - T_5$). Meteorological clouds should have positive ΔT (Yamanouchi et al. 1987), and volcanic plumes are expected to have negative ΔT (e.g., Prata 1989). Class separation, however, is especially difficult as ΔT approaches zero (Simpson et al. 2002). In fact, volcanoes with low levels of silicate in their plumes [e.g., Soufriere Hills (Montserrat), Bogoslof (Alaska), or White Island (New Zealand)] are especially difficult to differentiate from meteorological clouds (Simpson et al. 2001). Other factors [atmospheric water vapor, ice, chemical composition and particle size distribution, particle shape (departure from spherical), errors in radiometric calibration, surface emissivity, groundwater and juvenile water in the magma, optically active coatings (e.g., sulfuric acid)] also may compromise accurate detection using the split-window technique (also see Simpson et al. 2000, 2001; Pieri et al. 2002, and the references contained therein).

b. TOMS retrievals of total ozone, sulfur dioxide, and UV absorbing aerosols

The Total Ozone Mapping Spectrometer (TOMS) is an ultraviolet (UV) spectrophotometer (Heath et al. 1975). Six fixed wavelength bands in the 312–380-nm spectral region are used to measure the total ozone by differential absorption in the near-ultraviolet Huggins bands of ozone. Total ozone is in atmosphere-centimeters, multiplied by 100, and is reported as Dobson units. The instantaneous field of view of TOMS is 3° $\times$ 3°, which yields a 50 km $\times$ 50 km pixel at nadir.

The spectral contrast anomaly method, generally called the residue method, is the basis for TOMS total ozone retrieval (McPeters et al. 1996). The retrieval depends on a theoretical calculation [the Lambert-equivalent reflectivity (LER method)] of the backscattered ultraviolet (buv) radiation using the multiple-scattering radiative transfer model of Dave and Mateer (1967). The buv technique uses a pair of wavelengths (one ozone sensitive; the other ozone insensitive) to compute total ozone. The retrieval requires accurate separation of the spectral contrast (ratio of radiances at selected wavelengths) caused by ozone absorption from that caused by all other effects (Torres et al. 1998). The LER method provides the required separation.

Krueger et al. (1995) developed a TOMS sulfur dioxide (SO_2) index (SOI). This retrieval provides a way to track SO_2 plumes associated with volcanic eruptions (e.g., Krueger 1983; Seftor et al. 1997) and corrects TOMS total ozone when SO_2 is present (i.e., SO_2 can incorrectly enhance TOMS ozone, if not corrected). Krueger et al. (1995) recognized that the residue method can fail because of water clouds underlying a volcanic plume. To mitigate this problem, they adopted the in situ technique of Kerr et al. (1980) to operational processing of the satellite data.

The TOMS aerosol retrieval for *Nimbus-7* combines two independent pieces of information, the I_{340}/I_{380} spectral contrast and the change in backscattered 380-nm radiance, to detect the presence of absorbing and nonabsorbing particles embedded in the Rayleigh scattering atmosphere (Herman et al. 1997). Here, I_λ is either a measured backscattered radiance at a given wavelength or the corresponding radiance calculated using Dave's (1978) modified LER model. Both are used in the retrieval. The effects of clouds on spectral contrast are removed using the LER modified model (Herman et al. 1997). These wavelengths are not sensitive to total ozone. The spectral contrast for a fixed 380-nm radiance is largest for nonabsorbing aerosols/clouds and decreases with increasing absorption. The UV-absorbing aerosols (e.g., silicaceous aerosols, such as typical desert dust) produce smaller contrast than predicted by the LER technique, thereby producing positive residues. Nonabsorbing aerosols produce greater contrast and hence negative residues. Because clouds produce nearly zero residue, subpixel clouds do not affect the TOMS retrieval of aerosols. Aerosols detected would be reduced, however, because of obstruction of the aerosol layer by clouds [see Herman et al. (1997) and Torres et al. (1998) for details]. These residues constitute a dimensionless aerosol index.

Earth Probe Satellite TOMS algorithms for aerosol and SO_2 are based on the *Nimbus-7* retrieval described above. However, the 360-nm wavelength is used instead of 380 nm for reflectivity and 322- and 331-nm data are used instead of 331- and 340-nm data for the ozone retrieval. Details of the two computational procedures are given in the *Nimbus-7* and Earth Probe TOMS user's guides, respectively (McPeters et al. 1996, 1998).

3. Analyses of selected Asian dust events

''Yellow sand'' meteorological conditions (e.g., known as huangsha in China, whangsa in Korea, and kosa in Japan) occur in springtime throughout east Asia (Husar et al. 2001). The arid deserts of Mongolia and China are the source of the dust (Zheng et al. 1998).

The Asian dust events of April 2001 and April 1998 were selected for analysis because they are represen-

tative of similar historical events. Special emphasis is given to the April 2001 event because little about it has appeared in the literature to date. Representative results for the April 1998 event demonstrate that it is an analog of the April 2001 event. See the recent *Journal of Geophysical Research* special issue (2001, vol. 106, No. D16) for details of the April 1998 event.

a. The April 2001 dust event

1) SATELLITE EVIDENCE AND TIME LINE

A time series of the TOMS aerosol index (Figs. 1a–h) shows the evolution and dispersion of silicate dust from its east Asia source, across the Pacific basin, and into North American airspace from 7 to 14 April 2001. Aerosol index values as high as 2–3 characterize the dust cloud; these values are about 5 times as high as the background aerosol values observed by TOMS. Selected TOMS SO_2 retrievals (Figs. 1i,j), contemporaneous with the TOMS aerosol retrievals, show a very low SO_2 background level globally. These data are typical of all TOMS SO_2 observations for 7–14 April 2001. Together, the TOMS aerosol and SO_2 distributions show that the airborne dust is not volcanic. In addition, no eruption of significance was reported by the Global Volcanism Network during this time.

After 13 April 2001, the TOMS aerosol index begins to show smaller values. Several reasons potentially account for this fact. TOMS is primarily a stratospheric instrument and may not respond well to aerosols as they move into the troposphere. Settling and atmospheric dispersion over time reduce absolute concentration and, hence, the aerosol index.

A temporal composite (Fig. 2a) of the centroid(s) of the TOMS aerosol time series (Fig. 1) shows the spatial and temporal evolution of the main component of dust associated with this event. Atmospheric transport of the dust carried it into many regions of active volcanism (e.g., the Kuril/Kamchatka/Aleutian volcanic chains, the Indonesian archipelago). Major commercial and civilian aviation routes occur over the same regions. The pattern of dust over Africa (Fig. 2b) is associated with a separate Saharan dust event.

2) METEOROLOGICAL CONDITIONS

Asian dust is transported over the North Pacific Ocean by midlatitude westerlies and may cover the entire North Pacific area (Merrill et al. 1989, 1997). Substantial interannual variability occurs in peak concentration and in the extent to which individual dust events affect specific areas, that is, the Kuril/Kamchatka/Aleutian region (Prospero et al. 1989).

Large-scale patterns in sea level pressure during the April 2001 dust event [0000 UTC National Centers for Environmental Prediction (NCEP) Pacific surface analysis] show 1) the cyclonic center located along the eastern Asian coast, 2) the merging of the east and west Pacific anticyclonic centers into one strong high pressure center ($>$1035 hPa) in the central North Pacific, and 3) a deep low pressure center located along the Pacific Northwest coast (Figs. 3 and 4). These pressure fields produced a strong cyclonic flow of continental air from China that split into two distinct paths. One path was northeastward and across the Kamchatka Peninsula, along the Aleutians, and then southeastward into the Pacific Northwest. The other path was eastward across the Pacific and over the west and southwest coast of the United States. Aloft, the large-scale patterns at the 500-hPa level during the April 2001 dust event (0000 UTC NCEP Northern Hemisphere analysis) show 1) a large-scale north–south-oriented cold trough along the eastern Asian coast on 6 April 2001 that slowly drifts eastward into the Gulf of Alaska by 14 April 2001 (Fig. 5) and 2) a deep low located along the Pacific Northwest coast that began development on 12 April 2001.

The circulation associated with the cold trough resulted in strong anticlockwise flow aloft of continental air from China, which then flowed eastward across the Pacific into the Pacific Northwest. A secondary path involved the entrainment of some of the eastward flow into the eastern side of the trough moving northeastward into Kamchatka, the Aleutians, and mainland Alaska. This split flow is similar to the surface circulation described above (Figs. 3 and 4). The cold-core surface highs were shallow features in which the clockwise circulation weakened with altitude and in some areas reversed with the presence of the trough. This split transport system (Figs. 3 and 4) is consistent with the aerosol centroid movement observed in the TOMS data (Figure 2a). Sea-Viewing Wide Field-of-View Sensor (SeaWiFS) data (Figure 6) show the dust moving east and southeast behind a cold front consistent with the flow into the Pacific Northwest.

The cyclonic system over China for the April 2001 event was very deep (center pressure of $\sim$980 hPa) with strong winds (see Fig. 3e). The dynamic vertical forcing associated with this storm must have been very strong, lifting the dust well into the atmosphere ($>$5 km). Temperatures in March/April were too cold over China and the Asian coast for convection to play any significant role in vertical transport. For the dust to remain in the atmosphere and to be transported across the Pacific, it must travel in precipitation-free air. Wet deposition would otherwise remove most of it near its source region or before it reached North America. Thus, the dust must have reached nearly maximum height in the early stages of the storm over the desert. Moreover, the Gobi and Mongolian Deserts, source regions of the dust, are about 3 km above sea level (Rand McNally 1974). This elevation contributes to the ultimate atmospheric height reached by the dust (Fig. 5). The same conditions occurred during the 1998 event (e.g., Husar et al. 2001 and other references in the same volume).

An offshore low developed off of the Pacific North-

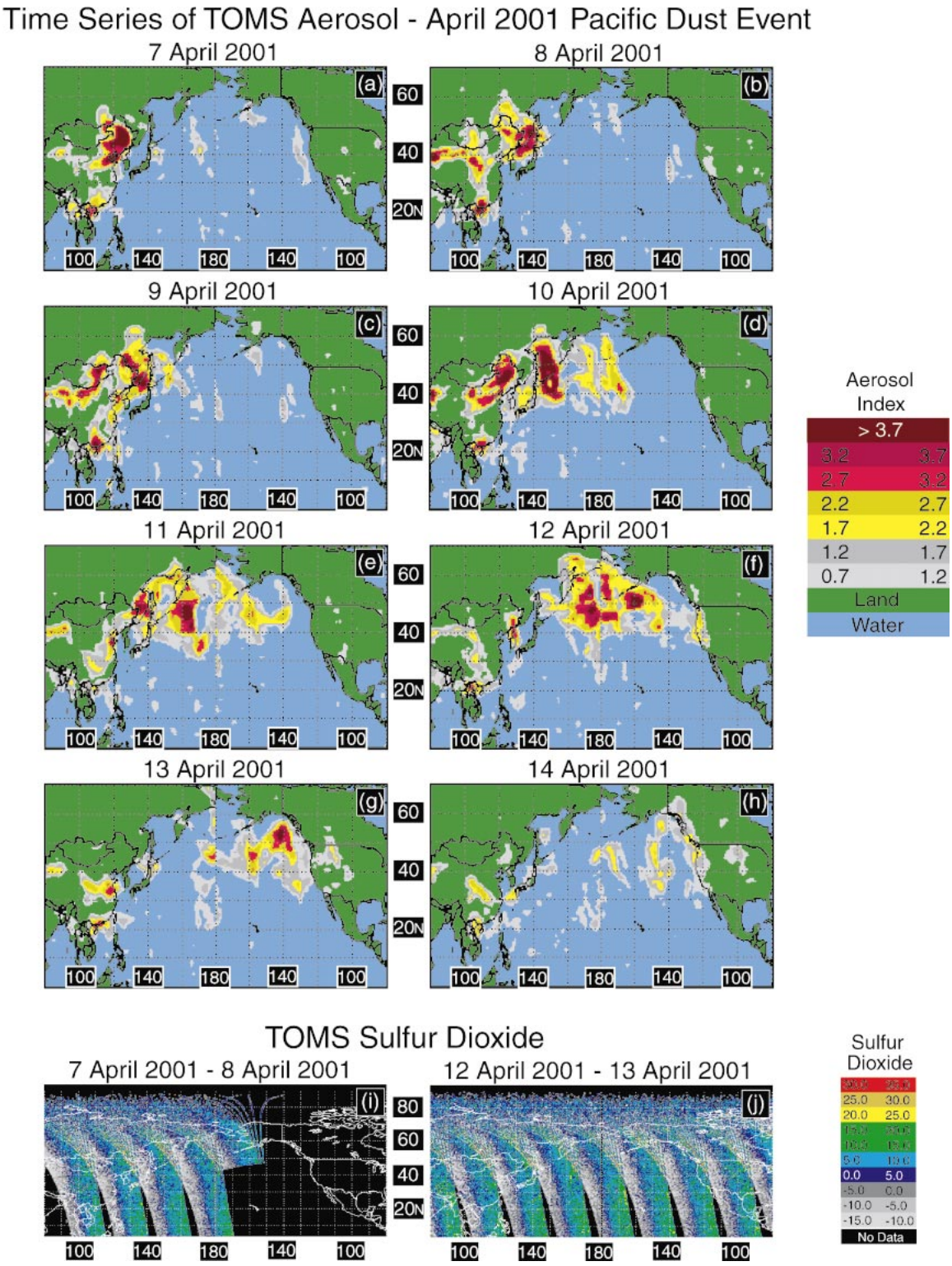

FIG. 1. (a)–(h) Sequence of TOMS aerosol index. (i), (j) Representative TOMS SO_2 data, which show little atmospheric SO_2. Data show the aerosol is nonvolcanic.

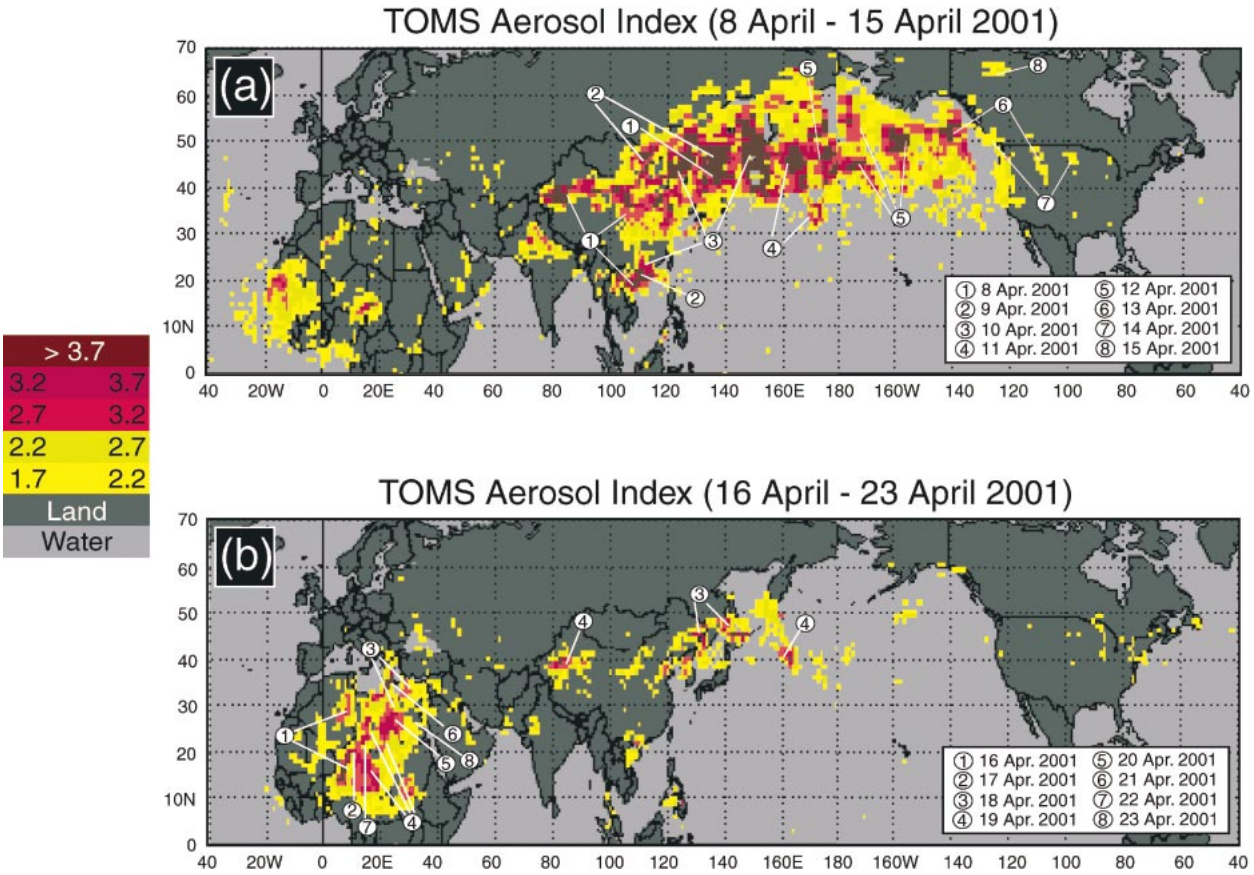

FIG. 2. Composite of TOMS aerosol data (Fig. 1) showing the dispersion of the aerosol centroid from its east Asian source, across the Pacific basin, and over North America.

west, starting around 14 April 2001. The resulting cyclonic offshore flow essentially shut off the northern transport route of dust into the Pacific Northwest for the April 2001 event but enhanced the southern path over the West Coast.

3) NUMERICAL SIMULATIONS

The Canadian Emergency Response Model (CANERM) was used in real time to model the long-range transport of Asian dust to North America. It is a three-dimensional Eulerian model (Pudykiewicz 1988; CMC 2002a) for medium- to long-range atmospheric transport of pollutants (e.g., volcanic ash). It is used when the space–time structure of the wind is complex or when the release of the pollutant occurs over time. The source of emission is modeled as a virtual source (Pudykiewicz 1989). It accounts for subgrid-scale effects near the point of release and is implemented as a 3D Gaussian function. Simulations compare well to data from field experiments (D'Amours 1998). The operational version used at the Canadian Meteorological Centre (CMC) has 25 vertical levels and a horizontal grid spacing of 5–150 km.

Meteorological data used by CANERM are provided by the CMC global data assimilation and forecasts systems (CMC 2002b). As is often the case, little quantitative data on the dust cloud were available in real time for the initialization of CANERM. The exact maximum altitude reached by the dust is unknown. There are indications that the dust was present, at least in small amounts, in the high troposphere and that it may even have reached the lower stratosphere (M. Fromm, Naval Research Laboratory, 2002, personal communication). The bulk of the dust, however, remained in the lower troposphere. Simulations of the April 2001 Asian dust event were produced using the following best-guess initial conditions: 1) the location of the northernmost centroid at 1200 UTC 8 April 2001 is 45°N, 137°E based on TOMS aerosol data (Fig. 1), 2) the horizontal grid is 150 km, 3) the horizontal distribution at the source is Gaussian with a standard deviation of one grid point, 4) the vertical distribution at the source is constant from the surface to 5 km, 5) the total mass of dust is 10^{11} kg, and 6) the event duration is 1 h. These simulation parameters define the quasi-instantaneous position and distribution of the dust cloud at 1200 UTC 8 April 2001.

Trajectories depicting the ''visual aerosol dust cloud''

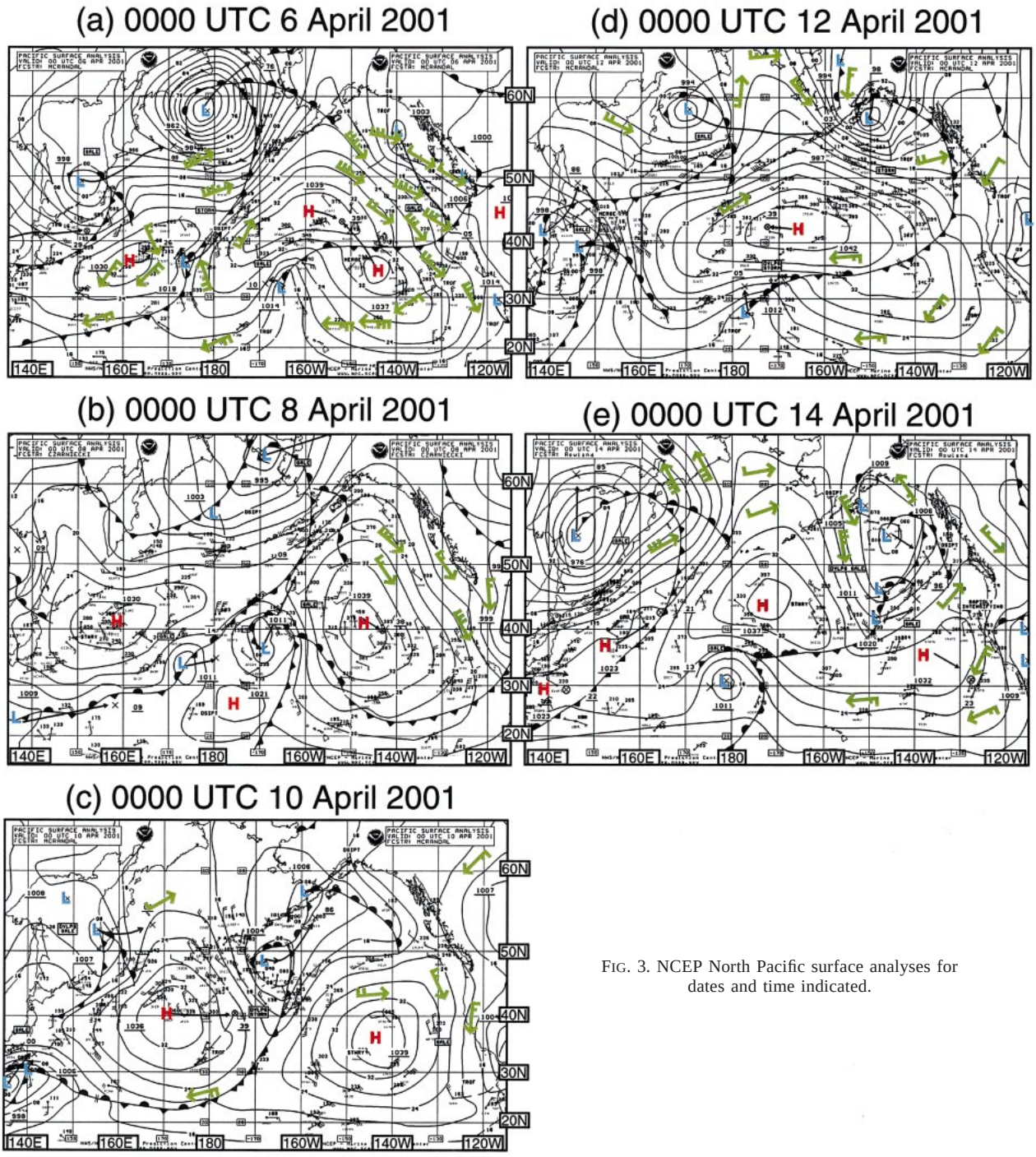

FIG. 3. NCEP North Pacific surface analyses for dates and time indicated.

were computed with CANERM for three flight-level ranges: surface–FL200 (~6.1 km), FL200–FL350 (~10.7 km), and FL350–FL600 (~18.2 km). This approach is analogous to what is done for the ''visual volcanic ash cloud'' as defined in ICAO (1998). Note that there is no internationally accepted definition of visual aerosol dust cloud. A single value for all situations does not exist. In a specific situation, the value is likely to change in time and space. This situation is especially true for a long-lived event in which the atmospheric transport would disperse the aerosols over a large domain. The problem is compounded by the uncertainty in the source term. For CANERM, a threshold value defining this quantity (100 μg m^{-3} average layer aerosol dust density) was used based on modeling studies of the visual volcanic ash cloud for the 1992 eruption

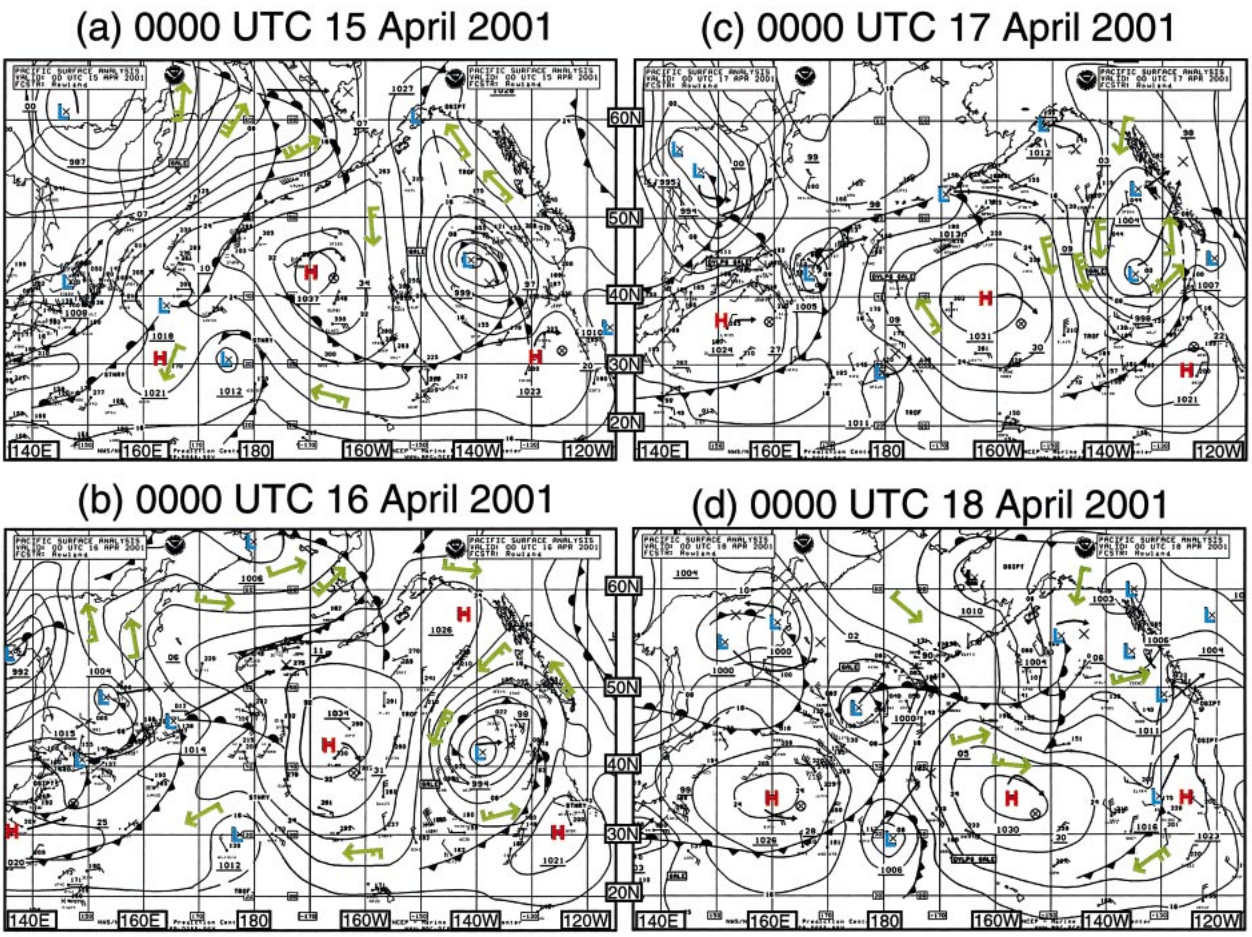

FIG. 4. Continuation of the sequence (Fig. 3) showing the blocking low.

of Mount Spurr in Alaska (USGS 1995). Little aerosol dust cloud appeared above FL350 in the simulations; these results are not shown.

Time series of the CANERM forecast of the aerosol dust cloud for the April 2001 event for surface–FL200 and for FL200–FL350 from 8 to 16 April 2001 (Figs. 7a,b) show that the areas of highest concentration agree reasonably well with the centroids of the TOMS aerosol data (Fig. 2a). Both sets of data indicate two paths of dust transport: one north over the Kuril/Kamchatka/Aleutian region into Alaska and then southward over North America and the eastern Pacific, and the other over the south-central Pacific basin toward North America. The CANERM results also suggest that the eastward transport of dust over Canada from the more northern stream was slowed considerably by a large blocking high centered near 66°N, 118°W. Dust, however, quickly continued toward North America from the more southerly route. Independent evidence (from lidar, satellite, and human observations) indicates that the dust traveled over the upper continental United States and lower parts of Canada, eventually reaching the east coast of North America and the western Atlantic Ocean. [At the time of writing, Asian dust imagery was available online at http://visibleearth.nasa.gov/Atmosphere/Aerosols/Dust_Ash.html and http://toms.gsfc.nasa.gov/aerosols/aerosols.html (TOMS aerosol search engine for dust events)]. Data from NOAA's polar-orbiting satellites at 1230 UTC 14 April 2001 show that the Asian dust was transported around the blocking high in western Canada and that it reached the western shore of Hudson Bay as well as the northern portions of Manitoba and Saskatchewan. The path and location are suggested by CANERM (Fig. 7). The transport of dust predicted by CANERM also is consistent with the large-scale pressure system (Figs. 3, 4, and 5).

A second CANERM run used the same initial conditions described above but with a constant vertical distribution between the surface and 10 km. The results for FL200–FL350, not shown here, do not match the TOMS data as well as do those of the first model run. Although considerable uncertainty remains, this result supports the hypothesis that most of the dust was found in the lower troposphere. The high desert surface source of the dust and the strong dynamical vertical forcing associated with the very deep low over China during the April 2001 event accounted for the initial lifting of

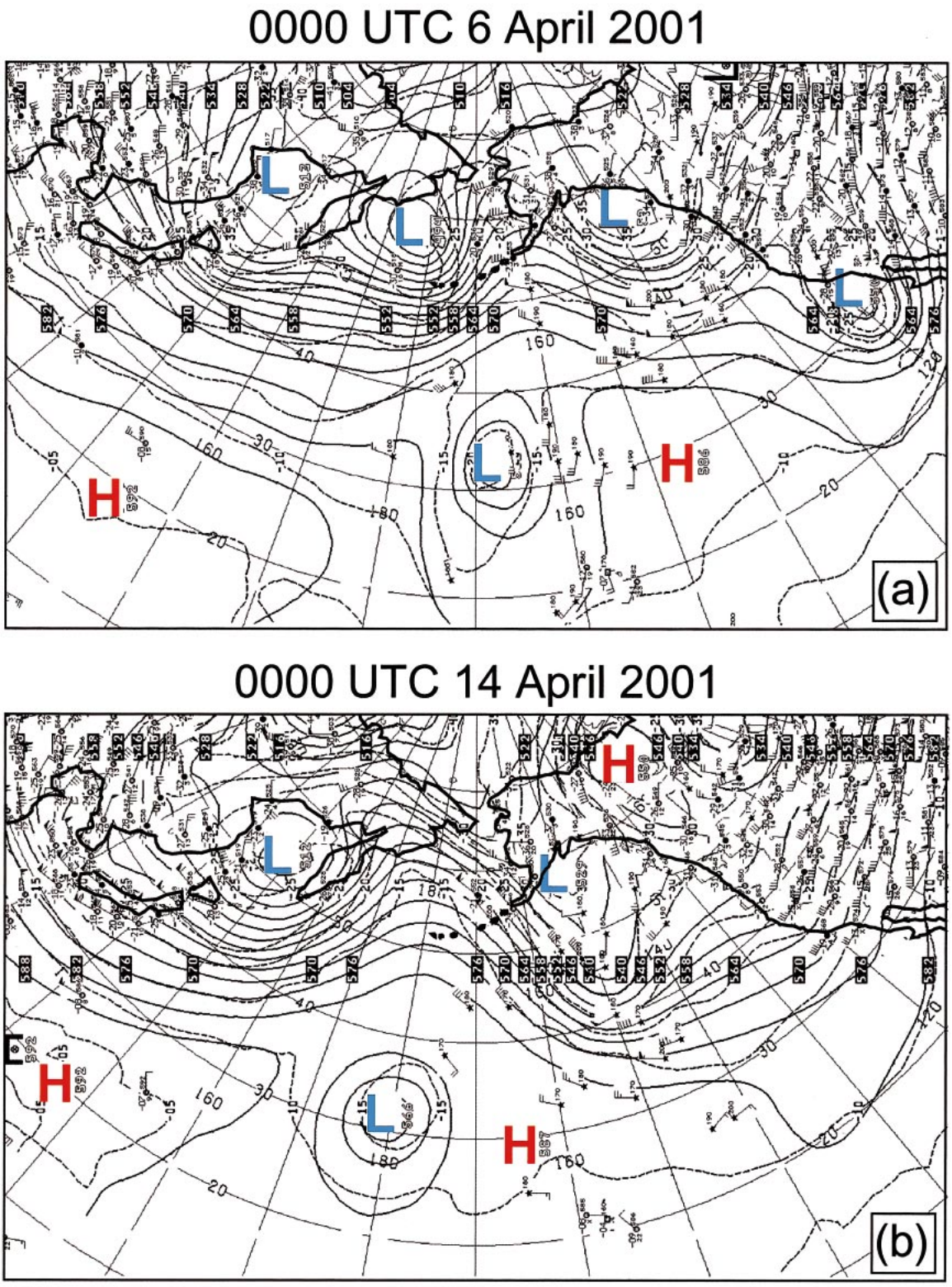

FIG. 5. Analogous to Fig. 4 but at the 500-hPa level.

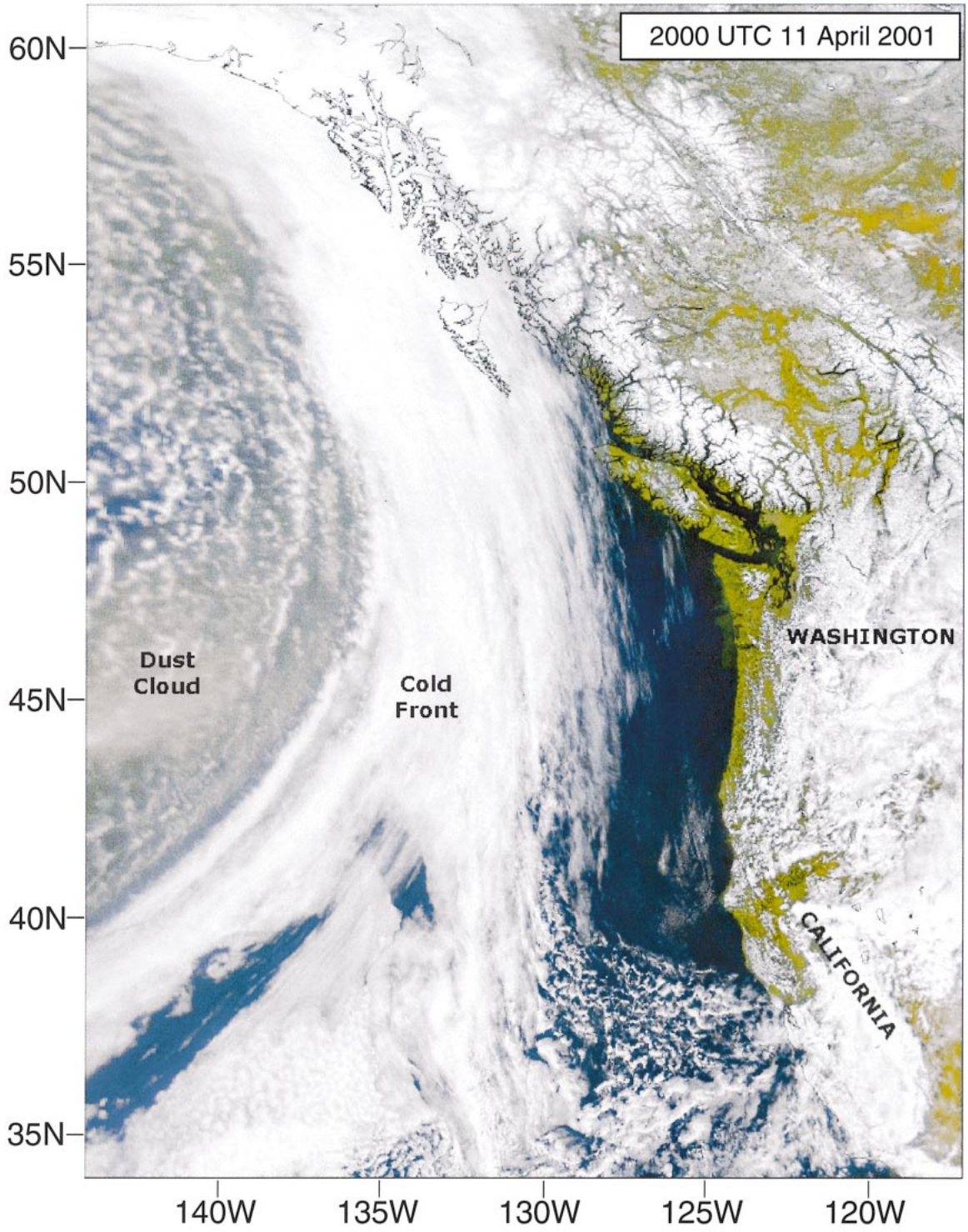

FIG. 6. SeaWiFS image of Asian dust off of the Pacific Northwest coast behind a cold front.

the dust into the atmosphere. However, trajectories (not shown here) indicate that beyond the first 24–36 h, the dust moved away from the influence of the low. From that point in time, the dynamical vertical forcing produced quasi-horizontal and even, later, subsiding flow. This is consistent with the CANERM simulations that show that the majority of the dust remained at relative low levels (surface–FL200).

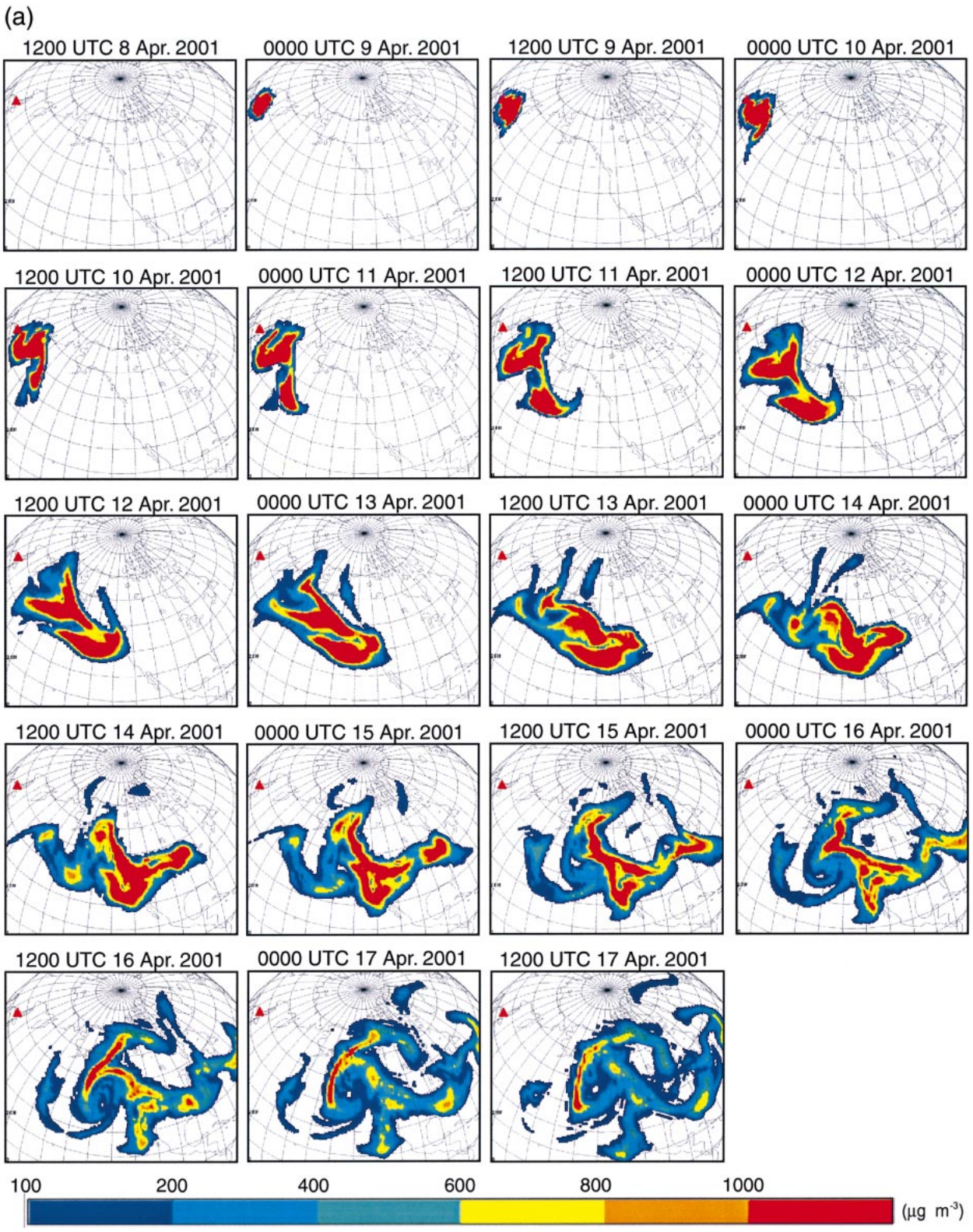

FIG. 7. Sequence of CANERM visual aerosol dust cloud layers from (a) the surface to FL200 and from (b) FL200 to FL350. Dates and times indicate time step of simulation.

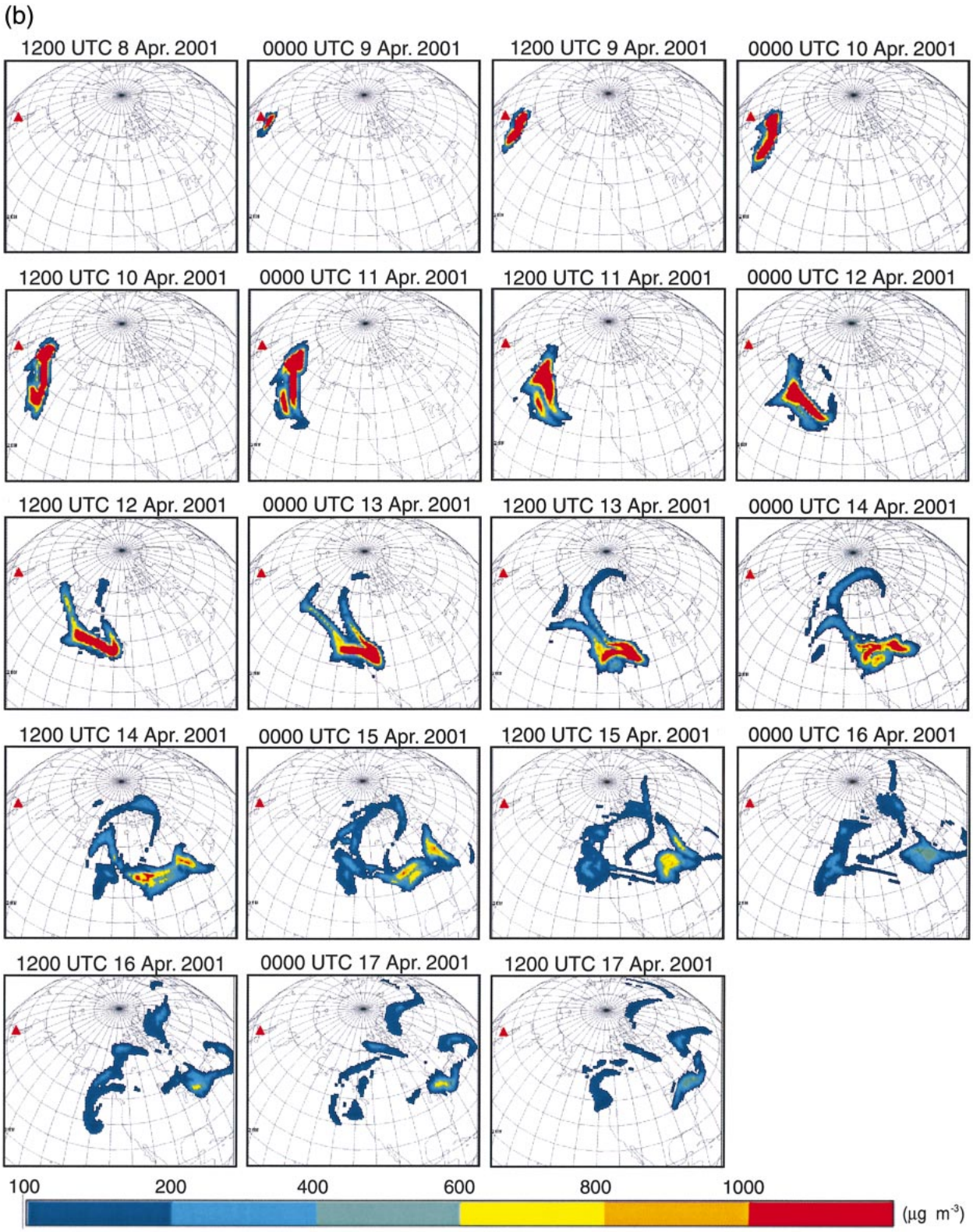

FIG. 7. (*Continued*)

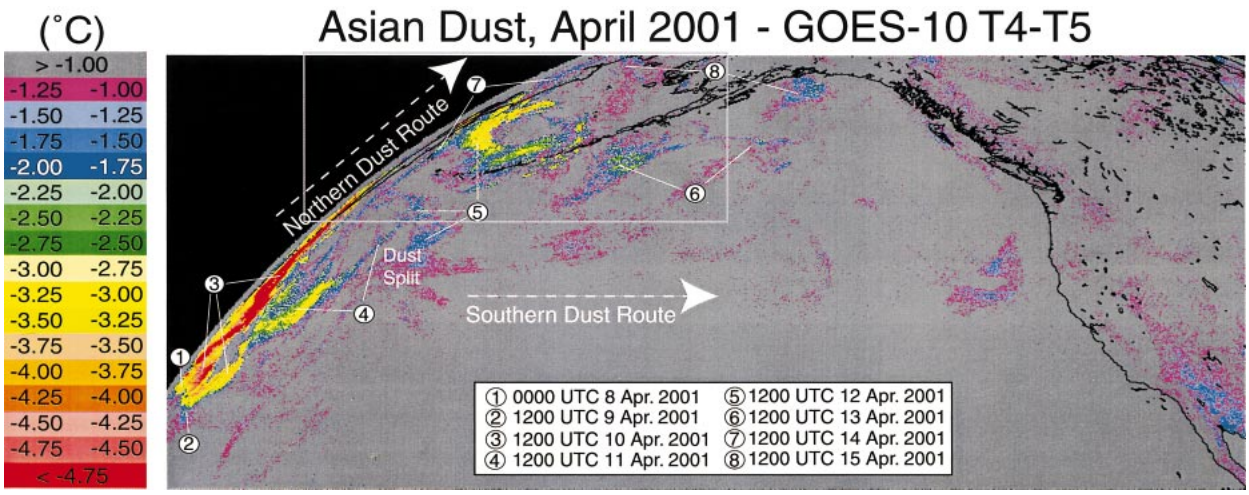

FIG. 8. Temporal composite of *GOES-10* $T_4 - T_5$ signatures showing dust movement; negative values imply dust or volcanic ash. The white box indicates region shown in Fig. 9.

In some instances, the CANERM model densities do not drop off as rapidly as in the TOMS data (Fig. 1). Several factors may contribute to this discrepancy: 1) inadequacies in the dry (and wet) deposition model formulation in CANERM, which is a fairly common problem in models; 2) the fact that TOMS is designed to measure stratospheric ozone and aerosols, and so TOMS may not respond as well to aerosols as they move lower into the troposphere with time; and 3) a combination of the first two factors and other possible factors. The model results are not meant to reproduce features in the aerosol dust cloud quantatively. Uncertainties in the source term alone preclude this possibility. Rather, we show that the model provides an operationally useful qualitative assessment of the motion of the aerosol dust cloud.

4) THE $T_4 - T_5$ SIGNAL

A temporal composite of *GOES-10* $T_4 - T_5$ scenes for the period 8–15 April 2001 (Fig. 8) shows the transport of Asian dust in two distinct trajectories. One trajectory follows a northeastern path over Kamchatka toward the Aleutian Islands and then into Alaska. The other follows a more southeastern route across the Pacific toward the west coast of Canada and the continental United States. The numbers correspond to the date of a given GOES image used to make the composite. The white box delineates a region examined in detail (Fig. 9).

The 11-μm BT for 12 April 2001 (Fig. 9a) was taken at 1200 UTC. This image occurs about midway in the temporal composite (Fig. 8). Considerable cloud cover occurs in this scene. Clouds (water or ice) produce positive $T_4 - T_5$ values, whereas both Asian dust and volcanic ash produce negative values. The numbered white regions are reference markers for the remaining panels of data. The corresponding $T_4 - T_5$ difference image (Fig. 9b) shows a strong negative signature as would airborne volcanic ash over the Aleutian Islands (also see the appendix). TOMS aerosol index (Fig. 9c) and SOI (Figure 9d) data correspond to the *GOES-10* $T_4 - T_5$ data, but at a different time. Correlations between the $T_4 - T_5$ data and the TOMS aerosol and SO_2 distributions are 0.61 and 0.19, respectively. The value of 0.19 for the $T_4 - T_5$–TOMS SO_2 is about that for Gaussian noise. Sample standard deviations of the observed differences between $T_4 - T_5$ values and predicted values (based on linear regression of models of $T_4 - T_5$–TOMS aerosols and $T_4 - T_5$–TOMS SO_2) are about 0.4 and 0.7, respectively. These analyses support the conclusion that the $T_4 - T_5$ signal in the *GOES-10* data is associated with the silicate aerosols of nonvolcanic origin.

The high aerosol values (Fig. 9) are from the Asian dust. The relatively low values of SO_2 (Fig. 9) correspond to the typical featureless SO_2 patterns in TOMS data for this period (Figs. 1i,j). Low SO_2 is inconsistent with volcanic ash in the stratosphere, especially early after an explosive magmatic eruption, but the spatial separation of SO_2 and airborne volcanic ash plumes from the same eruption has occurred [e.g., the El Chichón 1982 eruption in Mexico; see Schneider et al. (1999)]. The large-scale low-level patterns in the SOI, however, most likely imply no volcanic activity because volcanic ash ejection into the atmosphere can be considered as a point source, at least in the early stages of an eruption. Moreover, no volcanic alerts were issued for the region during this time.

Several issues can affect the correlations between the TOMS aerosol index, the TOMS SOI, and GOES $T_4 - T_5$ values. TOMS aerosol retrieval corrects for meteorological clouds using the modified LER model. Cloud (water or ice) can interfere with detecting either Asian dust or volcanic ash in GOES data. Clouds produce a positive $T_4 - T_5$ and several of the numbered regions

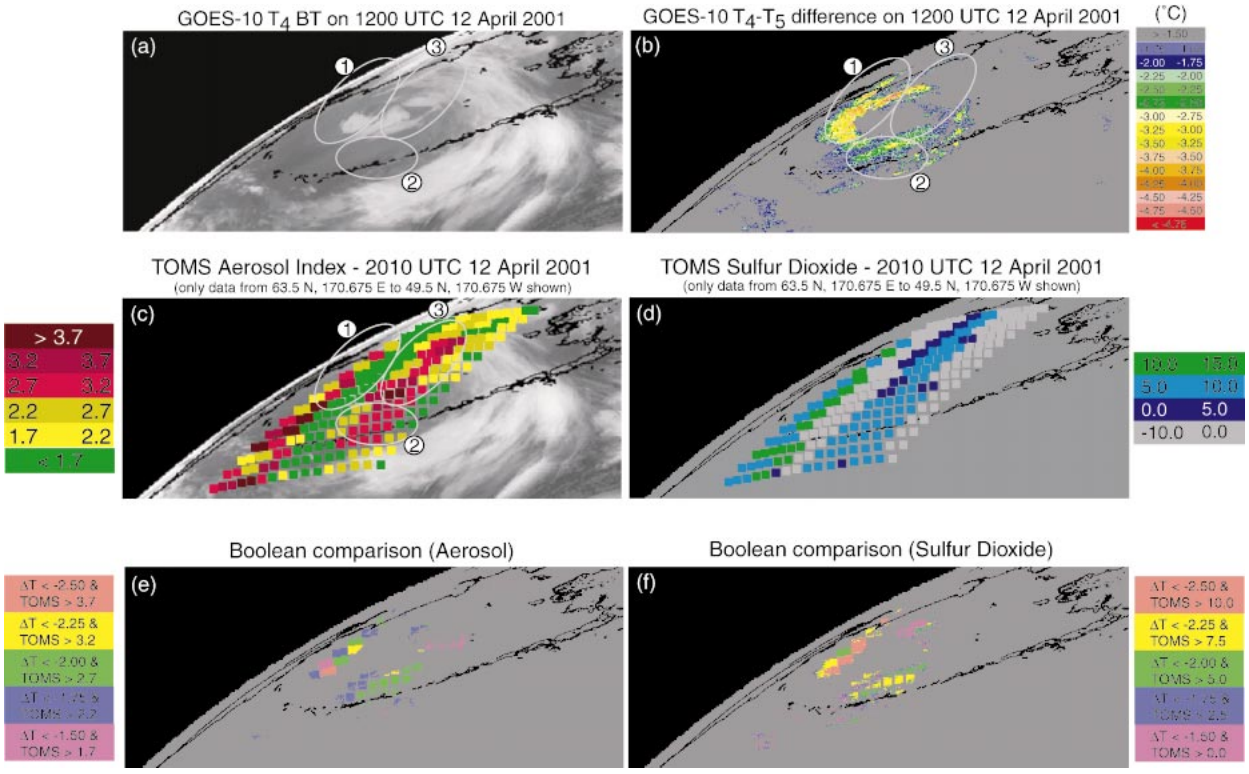

FIG. 9. *GOES-10* (a) 11-μm image of the Aleutians and (b) corresponding $T_4 - T_5$ signature; TOMS (c) aerosol and (d) SO_2. High aerosol/low SO_2 imply a nonvolcanic origin. Boolean comparison between $T_4 - T_5$ and TOMS (e) aerosol and (f) SO_2.

in Fig. 9a are cloud contaminated. GOES data (Fig. 9a) are an ''instantaneous'' snapshot (here night), whereas the TOMS data have an equator crossing time of 2010 UTC. Thus, there often is a significant time difference between the two. This, coupled with rapidly varying cloud cover, can exacerbate a comparison of the two types of data. The TOMS pixel is larger than the GOES pixel. GOES data, corresponding to a given TOMS pixel, were averaged. The mean $T_4 - T_5$ estimate is compared with the single TOMS pixel value.

Histograms of the TOMS global aerosol and SO_2 distributions for 12 April 2001 are shown in Figs. 10a and 10b, respectively. The inserts are histograms of the TOMS aerosol and SO_2 distributions for the region over the Aleutian Islands (Figs. 9c,d). The high-end tail values in the aerosol distribution indicate very high concentrations of absorbing silicate aerosol. These values are different from the corresponding global distribution. They represent the Asian dust reaching Alaska. The Alaskan TOMS SO_2 data, however, are very consistent with the global low SO_2 values. Again, a nonvolcanic origin of the silicate aerosol is supported.

b. The April 1998 dust event

1) SATELLITE DATA

Composite TOMS aerosol data (Fig. 11a) for the 16–26 April 1998 Asian dust event, analogous to the April 2001 event (Fig. 2a), show the transport of Asian dust across the Pacific. As with the April 2001 event, part of the dust moves northeast toward the Aleutian Islands and Alaska. A separate component of the dust moves southeast toward the continental United States and Canada. The corresponding GOES $T_4 - T_5$ temporal composite (Fig. 11b), analogous to that of the April 2001 event (Fig. 8), implies the transport of dust toward both the Aleutians/Alaska and the west coast of the United States and Canada. Values (central Pacific) are relatively low because of settling and dispersion processes while in transit. In situ data, however, confirm the arrival of dust off of southern California (e.g., Tratt et al. 2001). A separate outbreak of African dust from its Saharan source westward over the Atlantic is also shown.

The area of high aerosol index over the Gulf of Mexico (Fig. 11a) is not Asian or Saharan dust. In late March and early April of 1998, large fires developed in Mexico and Guatemala. TOMS also responds to carbonaceous aerosols (Torres et al. 1998).

2) METEOROLOGICAL CONDITIONS

Evolution of the 19–26 April 1998 Asian dust cloud over the Pacific Ocean was derived from a combination of SeaWiFS, *GOES-9* and *-10* images, and TOMS aerosol index data by Husar et al. (2001, their Fig. 3). The meteorological setting for this event had some similar

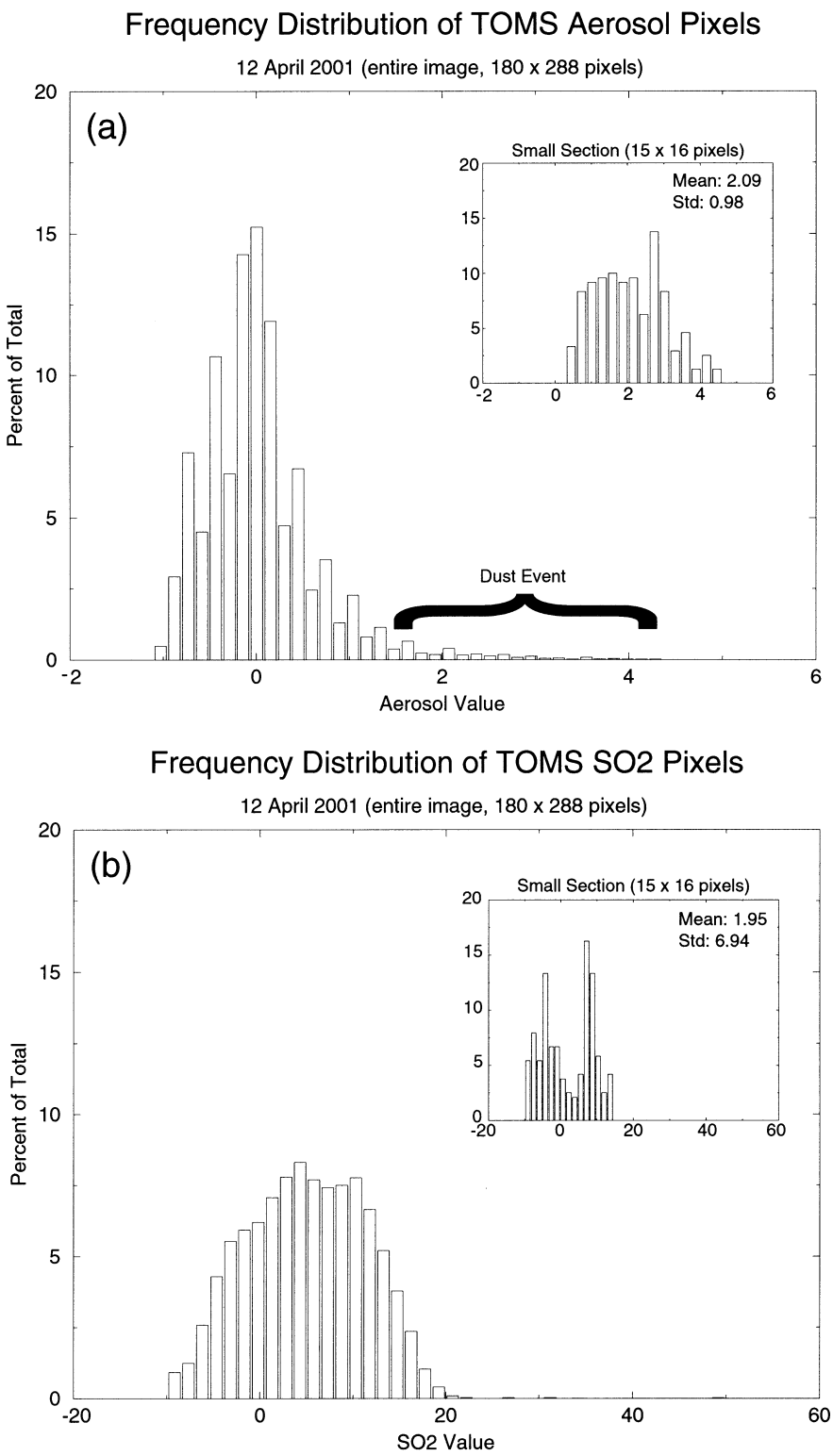

FIG. 10. Histograms of the global distribution of TOMS (a) aerosol and (b) SO_2 for 12 Apr 2001. Insets are for TOMS data over the Aleutian Islands (Figs. 9c,d).

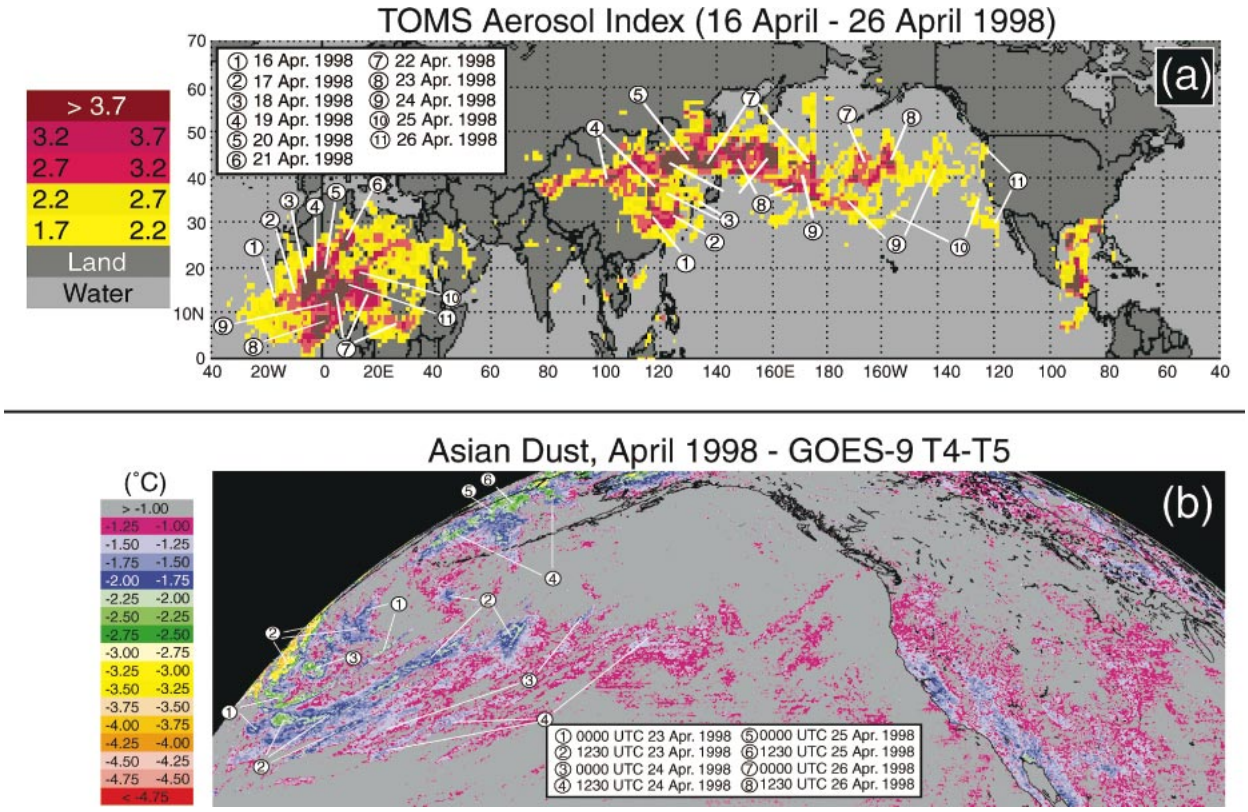

FIG. 11. Analogous to (a) Fig. 2 and (b) Fig. 8 but for Apr 1998.

features to the 2001 event but differed considerably over the far North Pacific.

Large-scale sea level pressure patterns for the 1998 dust event [0000 UTC NCEP Pacific surface analysis (Fig. 12)] similar to the 2001 event were 1) a cyclonic center located along the eastern Asian coast and 2) strong (>1030 hPa) east and west Pacific anticyclonic centers. Major differences with the 2001 event were that 1) the two anticyclonic centers did not merge into a single central Pacific center, 2) cyclonic centers were located across the far North Pacific Ocean, and 3) the large-scale circulation precluded the blocking of dust into the Pacific Northwest that occurred in 2001. The April 1998 500-hPa Northern Hemisphere analysis showed a different pattern than the 2001 event; there was a large-scale ridge over the surface deep lows in the northern Pacific and the Bering Sea that blocked northward flow of dust, keeping the transport farther south than in 2001 (D. Feit, Marine Prediction Center, NCEP, 2002, personal communication).

The pressure fields in 1998 resulted in strong cyclonic flow of continental air off of the China coast that moved northeastward over Korea into the North Pacific over the east Pacific high. There is no evidence of split flow over the central Pacific that occurred during April 2001. The effect of the deep lows in the far North Pacific was threefold: 1) the main dust cloud remained farther south than in 2001 as it was transported across the Pacific; 2) significant portions of the dust cloud were entrained northward into the deep lows, transporting dust into the Bering Sea on 21 April and into Alaska on 23 April; and 3) the large-scale circulation precluded the blocking of dust into the Pacific Northwest that occurred in 2001. This overall flow pattern in 1998 is substantiated in the satellite imagery in Fig. 11.

4. Discussion

a. The April 1998 and April 2001 Asian dust events

Satellite data (Figs. 1, 2, 8, and 11) show the transport of dust from its Asian desert sources across the Pacific during April of 1998 and 2001. During transport, the dust cloud is stretched longitudinally (Figs. 7, 11), consistent with the earlier findings of Husar et al. (2001) for the 19 April 1998 event. Bifurcation of the dust cloud occurred during both events. Part of the dust cloud travels eastward toward the western United States and Canada. Large fragments of the dust cloud, however, also are transported northeastward into the Arctic. This bifurcation is consistent with CANERM simulations of the dust transport for the 2001 event (Fig. 7) and with independent model simulations of the April 1998 event (Nickovic et al. 2001). However, details in the patterns of transport for the two events differ, as expected, given

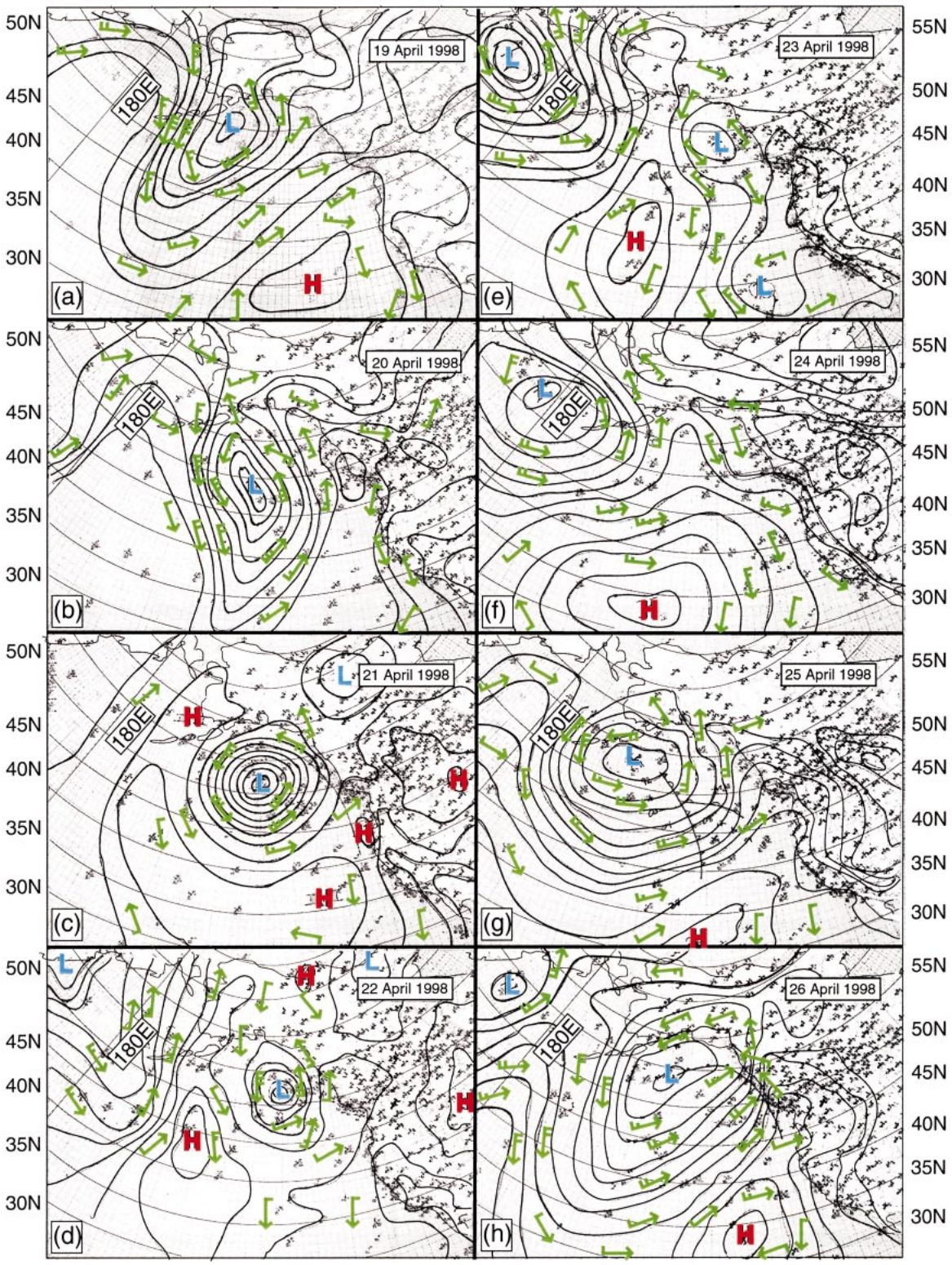

FIG. 12. Analogous to Figs. 3 and 4 but for Apr 1998.

the differences between the large-scale atmospheric circulations for the two events (Figs. 3, 4, and 12).

Dust from both events arrived over North America quickly. SeaWiFS data (Fig. 6) show dust from the 8 April 2001 event off of the west coast of Canada and the continental United States on 11 April 2001. Dust from the 19 April 1998 event was first observed at Salt Lake City, Utah, on 24 April 1998 using lidar, and the main dust cloud arrived on 25 April 1998 (Husar et al. 2001). The TOMS aerosol data for April 2001 (Fig. 1), the composite GOES $T_4 - T_5$ data (Fig. 8), and the CANERM simulations (Fig. 7) show that the dust cloud penetrated deep into North American airspace. Additional TOMS and CANERM data (not shown here) indicate that the dust eventually reached the east coast of North America and the western Atlantic Ocean. GOES data (Fig. 11b) support a similar conclusion for the 19 April 1998 event.

Gravitational Stokes settling (a dry removal process) usually occurs near the source within the first day of transport; it is effective at removing large-size (>10 μm) particles (Husar et al. 2001). Precipitation (a wet removal process) occurs sporadically throughout the 5–10-day lifetime of the remaining smaller-size particles. For dust to reach North America, little precipitation must occur while the dust crosses the Pacific. Data are not available from either event to establish precisely when the atmosphere was cleansed of the dust.

b. Particle size distribution and chemical composition

In situ data for the April 2001 event have not yet appeared in the literature. Therefore, we infer physical characteristics of Asian dust for this event using reported in situ observations for the April 1998 event. This method is justified given that the same source conditions and similar transport mechanisms/times occurred for both events.

Tratt et al. (2001) report a coarse-mode diameter range of 2–4 μm for dust from the 19 April 1998 event based on the inversion of sun and sky radiance measurements made at San Nicolas Island, California. Between 30% and 50% of the dust mass for this event was below 2.5 μm based on size-segregated dust samples taken at many isolated locations over the northwestern United States and Canada (McKendry et al. 2001). Based on such estimates, the aged Asian dust arriving at the North American west coast had a mass median diameter of 2–3 μm (Husar et al. 2001).

The 19 April 1998 event was preceded by a separate 15 April 1998 event. Chun et al. (2001a) analyzed the dust size distribution for this event based on observations made at Anmyon Island, Korea. It took 4 days for the dust to reach the island. The observed size distribution function has a sharp peak between 1 and 5 μm. with a volume-mean diameter of 2 μm and a logarithmic standard deviation of 1.6 μm. Moreover, there was a strong correlation between particles in the dust peak size range (2–3 μm), and there was almost no correlation with particles of less than 0.8 or of greater than 10 μm. The absence of large particles of greater than 10 μm is consistent with gravitational settling during its transit from the Gobi Desert to Anmyon Island.

Chun et al. (2001b) also compared aerosol concentration at Anmyon with those observed at Seoul, Korea. For the heavy dust period, the number size distributions of aerosols observed at both locations were characterized by decreases in small-size particles (<0.5 μm) and increases in large-size particles between 1.35 and 10 μm. The coarse particles were more affected by local sources.

Analyzed filter samples from the 19 April 1998 event that reached western Canada show the elemental signatures (silicon, iron, aluminum, and calcium) of a massive injection of lithic aerosols, with abundances of silicon approximately 2 times those previously recorded (McKendry et al. 2001). Ratios of these elements to iron are statistically similar to ratios observed in mineral aerosol events in Hawaii and China. Concentrations of PM10 are expressed in the weight of particulate matter (PM), centered around 10 μm in aerodynamic diameter, found in 1 m^3 of air [see Maynard and Walker (1996) for details]. In southern interior British Columbia, the PM10 levels increase dramatically to about 100 $\mu g\ m^{-3}$ on 28 April 1998 (Husar et al. 2001). The increased PM10 levels are consistent with mesoscale modeling of the 19 April 1998 Asian dust (McKendry et al. 2001): in fact, they conclude that it accounted for 40%–50% of the peak PM10 levels observed near Vancouver, British Columbia, Canada.

Tratt et al. (2001) tracked the three-dimensional structure of the Asian dust off of southern California using concurrent lidar data. The dust cloud was a well-developed multilayer structure (up to three layers) distributed throughout the free troposphere. The tropopause typically was at 10–11 km above mean sea level during these observations (see their Fig. 2). On 27 April 1998, for example, the dust layer was observed between 6- and 10-km height using lidar, with the backscattering more than 100 times the prevailing background levels.

c. Implications with respect to the detection of airborne volcanic ash

Asian dust, essentially a nonmafic aerosol of sedimentary origin transported by eolian processes, produces a split-window $T_4 - T_5$ signal similar to that of airborne volcanic ash detected by the algorithm of Prata (1989) and Rose et al. (1995). Moreover, the dust has the strong inverted arch- or U-shaped characteristic curve expected of volcanic ash (see the appendix). Gravitational settling quickly ($\sim$1 day) removes large dust particles (>10 μm) from the atmosphere. The residual peak particle size concentration (2–3 μm), combined with its high silica content, is the optimal condition for producing both of these volcanic-ash-like signatures.

Meteorologists need to recognize that Asian dust aerosols can also produce large negative $T_4 - T_5$ signals in 11- and 12-μm BT data (Figs. 8, 11b) and inverted arches (see the appendix and Fig. A1). Otherwise, dust could be misinterpreted as ''airborne volcanic ash'' by a VAAC and could potentially cause the incorrect issuing of a volcanic ash advisory statement (VAAS) to the community. Aviation warnings for dust storms or sandstorms are covered by significant meteorological information (SIGMET) reports issued by meteorological watch offices. There is currently no requirement for the VAACs to issue such advisories. Other factors (e.g., total precipitable water vapor or ice coating of the particles) may further complicate interpretation of the $T_4 - T_5$ signal (Simpson et al. 2000). Therefore, care should be exercised by VAACs to consider these problems.

Distinguishing between dust and volcanic ash can be helped by considering the typical area covered by the negative $T_4 - T_5$ signals, especially near its source region. Dust is lifted into the atmosphere by large-scale storms (area source); a volcanic ash cloud originates from what is essentially a point source, at least early on. Thus, an Asian dust cloud is likely to cover an area many orders of magnitude larger that a typical volcanic ash cloud. This criterion is qualitative but it may provide some help when trying to identify what is producing negative signals. Simultaneous use of TOMS aerosol and SO_2 indexes could help to mitigate this possibility. Large negative $T_4 - T_5$ values, a large positive TOMS aerosol index (>2), and a relatively low background TOMS SOI would suggest a nonvolcanic origin for the negative $T_4 - T_5$ signal. Lack of reported volcanic activity may also help to distinguish between dust and ash.

d. Potential effects on aviation

When turbine-engine aircraft encounter a cloud of solid aerosols, such as volcanic ash or airborne dust, ingestion of such particulates can cause various kinds of damage ranging from the scouring of forward-facing flight surfaces to the abrasion of internal engine parts to the clogging of critical cooling air passages deep within the engine (Casadevall 1992). The latter is particularly troublesome because it can cause surging, compressor-stall failure, and flameout with complete loss of thrust. For volcanic plumes, much of the ingested aerosol material is mafic volcanic glass. This material typically exhibits extrusion temperatures of 900°–1100°C (Williams and McBirney 1979), well within the range of turbofan ''turbine inlet temperatures,'' and thus readily melts, producing the observed clogging. In addition, more refractory mafic crystals are often found embedded within the glass (Predzepelski and Casadevall 1994).

A potentially similar hazard is posed by ingestion of airborne Asian dust. The provenance of material lofted from the Gobi and other Asian deserts represents a wide variety of lithologic environments from predominately sedimentary to igneous, including granitic and more mafic volcanics. Such material consists of polyphase particulates that range from individual refractory crystals (e.g., quartz and feldspars), which may have solidi well above 1000°C, as well as mineral and rock assemblages (e.g., granites and rhyolites) with solidi of less than 1000°C (Barker 1983). The glass transformation temperature (above which significant plastic translational mobility occurs in crystalline species) also is in the range of 700°–900°C for sodium, potassium, and calcium feldspars (Carmichael et al. 1974). Thus, for the Asian dust case, the full range of aircraft engine and hull abrasion and melting damage experienced in the purely volcanic case cannot be ruled out and, indeed, should be anticipated. In the future, highly efficient engines with exhaust inlet temperatures as high as 1500°–2000°C will increase the probability of grain melting, even for the most refractory crystalline aerosol components (Silski 2000).

Dust seepage into electronic bays could also have a variety of adverse effects, including increased operating temperatures. At the minimum, the dust may represent an additional maintenance cost. Moreover, pilots who encounter the dust at altitude may have difficulty distinguishing it from small-grained airborne volcanic ash. Hence, avoidance of the dust may be beneficial. Dust can also affect the operation of airports, especially in Asia. Early detection of advancing dust clouds would provide the lead time to develop operational alternatives should airport shutdowns be deemed necessary. Because the intermediate and long-term effects of Asian dust on aviation are largely unknown, additional studies are needed to clarify these issues.

e. Public health issues

Fine-particle concentrations (i.e., <2.5 μm in aerodynamic diameter: $PM_{2.5}$), unlike coarse particles, have been associated with increased mortality in several U.S. cities (Schwartz 1999). The toxicity of fine particles has been associated with their tendency to deposit in the alveolar region of the lung (U.S. Environmental Protection Agency 1995). By the time it reaches the west coast of North America, about 30%–50% of the dust mass has a diameter of 2.5 μm (McKendry et al. 2001). Thus, aged Asian dust represents a potential public health hazard, especially to people with chronic respiratory problems. Fine-grained volcanic ash poses similar risks. Dust can reach North America, however, only if little or no precipitation occurs while in transit over the Pacific.

Many meteorological and environmental agencies that operate VAACs also are mandated to provide information related to the issuance of ''air quality alerts.'' Both fine-grained Asian dust and airborne volcanic ash are potential public health hazards. The natures of their toxicities, however, are somewhat different, which is another compelling reason to distinguish nonvolcanic Asian dust from airborne volcanic ash properly.

5. Conclusions

The following conclusions are proposed.

1) Asian dust events, especially in springtime, occur frequently. Chinese National Academy records show that during the seventeenth century there were 0.3–1.0 sandstorms in Inner Mongolia per year, but by 1990 the annual rate had increased to 3.0–5.0 per year (information was found online at http://www.lakepowell.net/asiandust.htm). Multiple dust events occurred in January–May during 1997–2002 (information was found online at http://info.nies.go.jp:8094/kosapub).
2) Satellite and lidar observations clearly show transport of dust to the North Pacific atmosphere and over North America. Model results corroborate this result.
3) Large particles of dust do not reach North America because of gravitational settling.
4) Asian dust that reaches North America, with typical aerodynamic diameters of 2–3 μm, is derived largely from crustal rocks and minerals dominated by the elements silicon, iron, aluminum, and calcium.
5) The particle size distribution and chemical composition of the Asian dust are near optimal for producing a strong negative signal in the split-window $T_4 - T_5$ airborne volcanic ash detection algorithm used by most operational VAACs. An inverted arch characteristic of volcanic ash is also produced (see the appendix). Unless the VAAC meteorologists are trained to recognize and to interpret correctly these characteristics of Asian dust, a false VAAS could be issued. The misidentification of lofted dust versus volcanic ash has important operational impacts (potential false volcanic ash alert). Moreover, accurate and rapid detection of dust may help to warn flight operations in potentially affected airports about possible decreased visibility, especially in China, Korea, and Japan. It also has air safety (potential health) implications should dust get into the cabin.
6) Simultaneous use of TOMS aerosol and sulfur dioxide indexes with the $T_4 - T_5$ split-window retrieval can help to distinguish Asian dust from volcanic ash. TOMS data are unfortunately only available during daylight hours and may not be received in ''real time'' by some VAACs. The area covered by the negative $T_4 - T_5$ signals may also help to distinguish Asian dust from volcanic ash (the area is very large relative to that of a newly erupted volcanic ash plume, at least in the early stage).
7) Meteorological and environmental agencies that share responsibility for air quality advisories need to monitor the distribution of Asian dust because of its potential public health hazard.
8) Analogous dust events occur in other hyperarid regions (e.g., the Sahara).
9) The possible short- and long-term impacts of desert dust on aircraft should be examined and documented. Would these be significant enough to warrant the issuance of advisory messages by VAACs as is already the case for volcanic ash?
10) Experimental instruments [e.g., the Moderate Resolution Imaging Spectroradiometer (MODIS)] may prove useful, especially if TOMS data become unavailable.

6. Future plans

This study was presented at the International Operational Implications of Airborne Volcanic Ash: Detection, Avoidance and Mitigation Workshop (Anchorage, Alaska, May of 2002). Based on the response, we plan to make materials (e.g., satellite and simulation movie loops) available for incorporation into aviation training programs. Additional workshops at other locations also are being planned. Ongoing research efforts will be included in these future workshops.

Acknowledgments. The Scripps JIMO supported this work. JJS was supported by the University of California, San Diego. Jean-Philippe Gauthier and Serge Trudel, of CMC, developed the software to run, produce, and display the CANERM outputs. TOMS aerosol data were obtained from NASA (Dr. R. McPeters), sulfur dioxide data are from NOAA (Mr. G. Stevens) and NASA (Dr. R. McPeters), GOES data were provided by NOAA/NCDC, and TOVS profiles were provided by the University of Wisconsin. SeaWiFS data were obtained from the Naval Research Laboratory (Monterey, California) Web site (http://www.nrlmry.navy.mil/aerosol/Case_studies/20010413_epac). Support was also provided by the NASA Natural Hazards Applications Program at the Jet Propulsion Laboratory of the California Institute of Technology. Ryan Adams typed the manuscript. Two reviewers provided helpful comments.

APPENDIX

The Volcanic-Ash-Like Signature of Airborne Asian Dust

Asian dust produces a large negative $T_4 - T_5$ signature (Fig. A1a), and its $T_4 - T_5$ versus T_4 signature is the well-developed inverted arch or U shape (Figs. A1b,c) expected for volcanic ash (Prata 1989). By contrast, the $T_4 - T_5$ versus T_4 signatures of airborne volcanic ash associated with three known volcanic eruptions (Figs. A1d–f) are weaker or, in some cases, much weaker than the signature of Asian dust.

Assumptions of the $T_4 - T_5$ airborne volcanic ash detection algorithm (Prata 1989: Rose et al. 1995) explain this apparent paradox. The algorithm assumes a plane-parallel semitransparent plume layer with homogeneous physical properties. During the early stages of an eruption, these conditions generally are not sat-

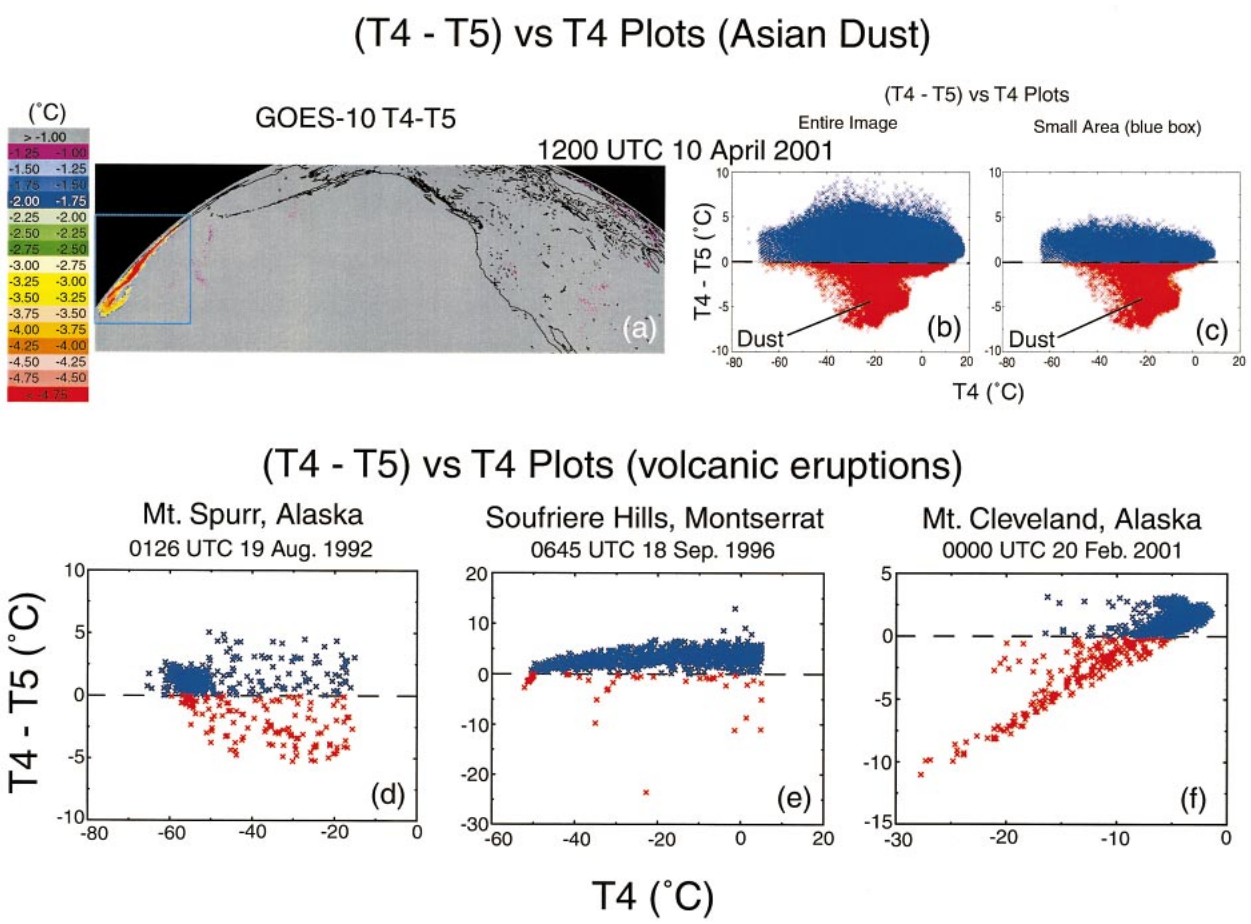

FIG. A1. (a) A representative GOES $T_4 - T_5$ Asian dust analysis, (b) $T_4 - T_5$ vs T_4 for all pixels in the scene, (c) analogous to (b) but for the area in the box, and (d)–(f) analogous to (c) but for the volcanic events indicated.

isfied by an ash plume. Asian dust distributions, however, more closely match these assumptions. The chemical composition of Asian dust is relatively simple and stable. By contrast, the chemical composition of a volcanic plume is complex and time varying. Moreover, eolian processes, over time, produce dust particles that are more spherical in shape than airborne volcanic ash (also see Pieri et al. 2002). Likewise, the particle size distribution of Asian dust has a sharp peak between 1and 5 μm, with a volume-mean diameter of 2 μm and a logarithmic standard deviation of 1.6 μm (Chun et al. 2001a). This, combined with the high silica content, produces near-optimal conditions for producing a strong negative signature, but not one of volcanic origin. By contrast, the particle size distribution and silica content of airborne volcanic ash have much more variability (they vary with eruption chemistry, etc.) The atmosphere also must be relatively dry for transport of Asian dust across the Pacific and over North America. Atmospheric moisture, juvenile water in magma, and groundwater entrained in the eruption plume greatly compromise the $T_4 - T_5$ detection of airborne volcanic ash [e.g., Fig. A1e; also see Simpson et al. (2000)].

REFERENCES

Bagnold, R. A., 1941: *The Physics of Blown Sand and Desert Dunes.* Methuen and Co., 265 pp.

Barker, D. S., 1983: *Igneous Rocks.* Prentice Hall, 416 pp.

Carmichael, I. S., F. J. Turner, and J. Verhoogen, 1974: *Igneous Petrology.* McGraw-Hill, 739 pp.

Casadevall, T. J., 1992: Volcanic hazards and aviation safety—Lessons of the past decade. *FAA Aviation Safety J.,* **2** (3), 9–17.

Chadwick, O. A., L. A. Derry, P. M. Vitousek, B. J. Huebert, and L. O. Hedin, 1999: Changing sources of minerals during four million years of ecosystem development. *Nature,* **397,** 491–497.

Chester, R. E., J. Sharples, G. S. Saunders, and A. C. Saydam, 1984: Saharan dust incursion over the Tyrrhenian Sea. *Atmos. Environ.,* **18,** 929–935.

Chun, Y., K. O. Boo, J. Kim, S.-U. Park, and M. Lee, 2001a: Synopsis, transport and physical characteristics of Asian dust in Korea. *J. Geophy. Res.,* **106,** 18 461–18 470.

——, J. Kim, J. C. Choi, K. O. Boo, S. N. Oh, and M. Lee, 2001b: Characteristic number size distribution of aerosol during Asian dust episode in Korea. *Atmos. Environ.,* **35,** 2715–2721.

CMC, cited 2002a: Atmospheric transport models for environment emergencies. Canadian Meteorological Centre. [Available online at http://gfx.weatheroffice.ec.gc.ca/cmc_library/data/PREVISIONS/e_8.pdf.]

——, cited 2002b: Global forecast system. Canadian Meteorological Centre. [Available online at http://www.smc-msc.ec.gc.ca/cmc/op_systems/global_forecast_e.html.]

D'Amours, R., 1998: Modeling the ETEX plumed dispersion with the Canadian Emergency Response Model. *Atmos. Environ.,* **32,** 4335–4341.

Dave, J. V., 1978: Effects of aerosols on the estimation of total ozone in an atmospheric column from the measurement of its ultraviolet observations. *J. Atmos. Sci.,* **35,** 899–911.

——, and C. L. Mateer, 1967: A preliminary study on the possibility of estimating total atmospheric ozone from satellite measurements. *J. Atmos. Sci.,* **24,** 414–427.

Dulac, F., D. Tanré, G. Bergametti, P. Buat-Menard, M. Desbois, and D. Sutton, 1992: Assessment of the African airborne dust mass over the western Mediterranean Sea using Meteosat data. *J. Geophys. Res.,* **97,** 2489–2506.

Gillette, D., 1978: A wind tunnel simulation of the erosion of soil: Effects of soil texture, sand-blasting, wind speed and soil consolidation on the dust production. *Atmos. Environ.,* **12,** 1735–1743.

Heath, D. F., A. J. Krueger, H. A. Roeder, and B. D. Henderson, 1975: The solar backscatter ultraviolet and total ozone mapping spectrometer (SBUV/TOMS) for Nimbus G. *Opt. Eng,* **14,** 323–331.

Herman, J. R., P. K. Bhartia, O. Torres, C. Hsu, C. Seftor, and E. Celarier, 1997: Global distribution of UV-absorbing aerosols from Nimbus7/TOMS data. *J. Geophys. Res.,* **102,** 16 911–16 922.

Husar, R. B., and Coauthors, 2001: Asian dust events of April 1998. *J. Geophys. Res.,* **106,** 18 317–18 330.

ICAO, 1998: Annex 3 to the Convention on International Civil Aviation (July 1998). Meteorological Service for International Air Navigation, International Civil Aviation Organization International Standards and Recommended Practices, ICAO, 92 pp.

Kerr, J. B., C. T. McElroy, and R. A. Olafson, 1980: Measurements of ozone with the Brewer ozone spectrophotometer. *Proc. Int. Ozone Symp.,* Vol. 1, Boulder, CO, NASA–NOAA–WMO, 74–79.

Krueger, A. J., 1983: Sighting of El Chichón sulphur dioxide clouds with the Nimbus-7 total ozone mapping spectrometer. *Science,* **220,** 1377–1379.

——, L. S. Walter, P. K. Bhartia, C. C. Schnetzler, N. A. Krotkov, I. Sprod, and G. J. S. Bluth, 1995: Volcanic sulfur dioxide measurements from the total ozone mapping spectrometer instruments. *J. Geophys. Res.,* **100,** 14 057–14 076.

Maynard, R. L., and R. Walker, 1996: Suspended particulate matter and health: New light on an old problem. *Thorox,* **51,** 1174–1176.

McKendry, I. G., J. P. Hacker, R. Stull, S. Sakiyama, D. Mignacca, and K. Reid, 2001: Long-range transport of Asian dust to the Lower Fraser Valley, British Columbia, Canada. *J. Geophys. Res.,* **106,** 18 361–18 370.

McPeters, R. D., and Coauthors, 1996: Nimbus-7 Total Ozone Mapping Spectrometer (TOMS) data products user's guide. NASA Ref. Publ. 1384, 73 pp.

——, and Coauthors, 1998: Earth Probe Total Ozone Mapping Spectrometer (TOMS) data products user's guide. NASA Tech. Publ. 1998-206895, 70 pp.

Merrill, J. T., M. Uematsu, and R. Bleck, 1989: Meteorological analysis of long range transport of mineral aerosol over the North Pacific. *J. Geophys. Res.,* **94,** 8584–8598.

——, R. E. Newell, and A. S. Bachneier, 1997: A meteorological overview of the Pacific Exploratory Mission West Phase B. *J. Geophys. Res.,* **102,** 28 241–28 253.

Myhre, G., and F. Stordal, 2001: Global sensitivity experiments of the radiative forcing due to mineral aerosols. *J. Geophys. Res.,* **106,** 18 193–18 204.

Nickovic, S., G. Kallos, A. Papadopoulus, and O. Kakaligou, 2001: Model for prediction of desert dust cycle in the atmosphere. *J. Geophy. Res.,* **106,** 18 113–18 130.

Ozloy, E., N. Kubilay, S. Nickovoc, and C. Moulin, 2001: An atmospheric dust storm affecting the Atlantic and Mediterranean in April 1994: Analysis, modeling, ground-based measurements and satellite observations. *J. Geophys. Res.,* **106,** 18 439–18 460.

Pieri, D., C. Ma, J. J. Simpson, G. Hufford, T. Grindle, and C. Grove, 2002: Analyses of in-situ airborne volcanic ash form the February 2000 eruption of Hekla Volcano, Iceland. *Geophys. Res. Lett.,* **29,** doi:10.1029/2001GL013688.

Prata, A. J., 1989: Infrared radiative transfer calculations for volcanic ash clouds. *Geophys. Res. Lett.,* **16,** 1293–1296.

Predzepelski, Z. J., and T. J. Casadevall, 1994: Impact of volcanic ash from 15 December 1989 Redoubt Volcano eruption on GE CF6-80C2 turbofan engines. *Volcanic Ash and Aviation Safety: Proceedings of the First International Symposium on Volcanic Ash and Aviation Safety,* T. J. Casadevall, Ed., U.S. Geologic Survey Bull. 2047, 129–135.

Prospero, J. M., M. Uematsu, and D. Savoic, 1989: Mineral aerosol transport to the Pacific Ocean. *Chemical Oceanography,* J. P. Reiley and R. Chester, Eds., Vol. 10, Academic Press, 187–218.

Pudykiewicz, J., 1988: Numerical simulation of the transport of radioactive cloud from the Chernobyl nuclear accident. *Tellus,* **40B,** 241–259.

——, 1989: Simulation of the Chernobyl dispersion with a 3-D hemispheric tracer model. *Tellus,* **41B,** 391–412.

Rand McNally, 1974: *The International Atlas.* Rand McNally and Co., 222 pp.

Rose, W. I., and Coauthors, 1995: Ice in the 1994 Rabaul eruption cloud: Implications for volcano hazard and atmospheric effects. *Nature,* **375,** 477–479.

Schneider, D. J., W. I. Rose, L. R. Coke, G. J. S. Bluth, I. E. Sprod, and A. J. Krueger, 1999: Early evolution of a stratospheric volcanic eruption cloud as observed with TOMS and AVHRR. *J. Geophys. Res.,* **104,** 4037–4050.

Schwartz, J., G. Norris, T. Larson, L. Sheppard, C. Claiborne, and J. Koenig, 1999: Episodes of high coarse particle concentrations are not associated with increased morality. *Environ. Health Perspec.,* **107,** 339–342.

Seftor, C. J., N. C. Hsu, J. R. Herman, P. K. Bhartia, O. Torres, W. I. Rose, D. J. Schneider, and N. Krotkov, 1997: Detection of volcanic ash clouds from Nimbus 7/total ozone mapping spectrometer. *J. Geophys. Res.,* **102,** 16 749–16 759.

Silski, C. L., 2000: Ultra-Efficient Engine (UEE) technology program due. *Commerce Business Daily,* PSA No. 2527, 1 February 2000.

Simpson, J. J., G. Hufford, D. Pieri, and J. Berg, 2000: Failures in detecting volcanic ash from a satellite-based technique. *Remote Sens. Environ.,* **72,** 191–217.

——, ——, ——, and ——, 2001: Response to ''Comments on 'Failures in detecting volcanic ash from a satellite-based technique'.'' *Remote Sens. Environ.,* **78,** 347–357.

——, ——, ——, R. Servranchx, J. S. Berg, and C. Bauer, 2002: The February 2001 eruption of Mount Cleveland, Alaska: Case study of an aviation hazard. *Wea. Forecasting,* **17,** 691–704.

Talbot, R. W., R. C. Harris, E. V. Browell, G. L. Gregory, D. I. Sebacher, and S. M. Beck, 1986: Distribution and geochemistry of aerosols in the tropical North Atlantic troposphere: Relationship to Saharan dust. *J. Geophys. Res.,* **91,** 5173–5182.

Torres, O., P. K. Bhartia, J. R. Herman, Z. Ahmad, and J. Gleason, 1998: Derivation of aerosol properties from satellite measurements of backscattered ultraviolet radiation: Theoretical basis. *J. Geophys. Res.,* **103,** 17 099–17 110.

Tratt, D. M., R. J. Frouin, and D. L. Westphal, 2001: April 1998 Asian dust event: A southern California perspective. *J. Geophys. Res.,* **106,** 18 371–18 379.

U.S. Environmental Protection Agency, 1995: On-site meteorological program guidance for regulatory modeling applications. EPA-450/4-87-013, Research Triangle Park, NC.

USGS, 1995: The 1992 eruptions of Crater Peak Vent, Mount Spurr Volcano, Alaska. USGS Bull. 2139, 220 pp.

Williams, H., and A. R. McBirney, 1979: *Volcanology.* Freeman, Cooper and Co., 397 pp.

Yamanouchi, T., K. Suzuki, and S. Kawaguchi, 1987: Detection of clouds in Antarctica from infrared multispectral data of AVHRR. *J. Meteor. Soc. Japan,* **65,** 949–961.

Zheng, X., F. Lu, X. Fang, Y. Fang, and L. Guo, 1998: A study of dust storms in China using satellite data. *Proc. SPIE,* **3501,** 163–168.